THE JOURNAL OF PHYSICAL CHEMISTRY A
A JOURNAL OF THE AMERICAN CHEMICAL SOCIETY

pubs.acs.org/JPCA

Article

Quantum Control of Atom-Ion Charge Exchange via Light-Induced Conical Intersections

Published as part of The Journal of Physical Chemistry virtual special issue "Cold Chemistry".

Hui Li, Ming Li, Alexander Petrov, Eite Tiesinga, and Svetlana Kotochigova*

Cite This: *J. Phys. Chem. A* 2023, 127, 5979−5985

Read Online

ACCESS | Metrics & More | Article Recommendations | Supporting Information

ABSTRACT: Conical intersections are crossing points or lines between two or more adiabatic electronic potential energy surfaces in the multidimensional coordinate space of colliding atoms and molecules. Conical intersections and corresponding nonadiabatic coupling can greatly affect molecular dynamics and chemical properties. In this paper, we predict significant or measurable nonadiabatic effects in an ultracold atom−ion charge-exchange reaction in the presence of laser-induced conical intersections (LICIs). We investigate the fundamental physics of these LICIs on molecular reactivity under unique conditions: those of relatively low laser intensity of 10^8 W/cm^2 and ultracold temperatures below 1 mK. We predict irregular interference effects in the charge-exchange rate coefficients between K and Ca^+ as functions of the laser frequency. These irregularities occur in our system due to the presence of two LICIs. To further elucidate the role of the LICIs on the reaction dynamics, we compare these rate coefficients with those computed for a system where the CIs have been "removed". In the laser frequency window, where conical interactions are present, the difference in rate coefficients can be as large as 1×10^{-9} cm^3/s.

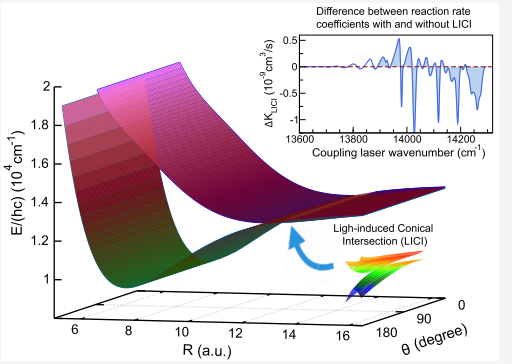

1. INTRODUCTION

Theoretical descriptions of many chemical processes are often based on the Born−Oppenheimer (BO) approximation.[1] This approximation relies on the observation that the motion of electrons and atomic nuclei occurs on different time or energy scales and thus allows the separation of electronic and nuclear degrees of freedom. The resulting model simplification minimizes computational efforts.

There exist, however, many cases where the coupling between electronic and nuclear motion is non-negligible and the BO approximation breaks down.[2] In particular, the potential energy surfaces of electronic states with the same symmetry of polyatomic molecules with three or more atoms can be degenerate at crossing points or curves in the multidimensional space of the nuclear coordinates. These crossings are called conical intersections (CIs). Generally, CIs form a seam of $3N - 8$ dimensions, where N is the number of atoms in the molecule. At these crossings, strong nonadiabatic transitions between electronic states occur.

Conical intersections between molecular electronic potential surfaces thus greatly affect the molecular dynamics and chemical reactivity. Conditions under which conical intersections occur have been extensively reviewed in refs 3−5. Naturally occurring CIs play a crucial role in photochemistry and photobiology as well as optical and superconductor physics.[3,6−8] Clearly, the location of such CIs and the strength of the related nonadiabatic couplings are inherent properties of the atoms in the molecule and are difficult to manipulate or control.

When molecules are exposed to resonant laser light, however, new features can emerge. Moiseyev et al.[9] showed that with laser light it is possible to create a conceptually different kind of CI even in diatomic molecules, a so-called light-induced conical intersection (LICI). In contrast to natural conical intersections, the characteristics of LICIs are easily modified by the parameters of the laser field. The internuclear positions of LICIs are determined by the laser frequency and the direction of the laser polarization ϵ. That is, the angle θ between a molecular axis and the direction of polarization adds a motional degree of freedom, and a controllable CI can appear.

Initial theoretical descriptions of LICIs[9−13] focused on the diatomic Na_2 molecule interacting with either a retroreflected laser beam creating a spatial standing wave potential for the dimer or with short but strong laser pulses. For both implementations this leads to a degeneracy of "dressed'

Received: January 11, 2023
Revised: June 26, 2023
Published: July 12, 2023

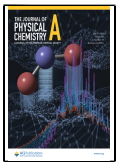

electronic states in a two-dimensional space, where one of the coordinates is the separation R between the sodium atoms. Study of the core excited CO* molecule in X-ray regimes[14,15] show that LICIs should lead to nonadiabatic transitions between electronic, vibrational, and rotational degrees of freedom of the diatomic molecule. In addition, with the ready availability of laser-cooled atoms there is also a growing interest in these concepts applied to ultracold atom−atom collision.[16−18] The dramatic effect of the light-induced conical intersection on the photodissociation and photofragmentation of the D_2^+ molecule was demonstrated in refs 19−21. Recently, Csehi et al.[22,23] in theoretical studies showed that LICI in diatomics can be created even by quantized radiation field in an optical cavity.

Light-induced conical intersections have been studied experimentally with ultrafast molecular processes. Kim et al.[24] found that a LICI can control the isomerization of 1,3-cyclohexadiene, while Corrales et al.[25] investigated the transition from weak to strong fields in the LICI-induced dissociation of polyatomic methyl iodide. Quantum interference in the dissociation of H_2^+ initiated by a LICI was observed by Natan et al.[26] with focused 30 fs laser pulses with a peak intensity of 2×10^{13} W/cm^2. Finally, Kübel et al.[27] performed detailed investigations of the light-induced molecular potentials in the same molecular system. They demonstrated the presence of distortions in the nonadiabatic potential energy surfaces from modulations in the angular distribution of the reaction paths.

Here, we investigate the role played by LICIs in the charge-exchange reaction between ground-state $^{40}Ca^+$ ions and neutral ground-state ^{39}K atoms prepared in well-controlled quantum states and at ultracold collision energies. We envision two experimental realizations of our ideas. The first corresponds to one where ultracold K and Ca^+ are stored in overlapping optical dipoles and Paul traps, respectively, and the frequency of a linearly polarized laser is tuned. In a dressed-state picture or with Floquet analysis, dressed molecular states satisfy the conditions required for LICIs as schematically shown in Figure 1. Two dressed adiabatic molecular states as functions of the atom−atom separation R and the angle between the interatomic axis and the laser polarization θ touch forming one or two LICIs at one or two pairs (R, θ). The nontrivial dependence of the charge-exchange rate coefficient on laser frequency can then reveal the presence of LICIs. Our simulations will be restricted to this realization.

A second realization, not studied here, to show the presence of LICIs might correspond to the case where spatially separate clouds of ultracold K and Ca^+ are accelerated toward each other to form a KCa^+ quasi-molecule with an oriented interatomic axis. In the presence of a linearly polarized laser, the behavior of the charge-exchange reaction rate as a function of the angle between the collision axis and the laser polarization direction can then reveal the presence of LICIs. Prototype experiments studying oriented collisions between two ultracold neutral atom clouds can be found in ref 28.

Our model of the former realization allows us to investigate the effect of multiple "pathways" around the two LICIs that occur in our system. These pathways lead to interference patterns in the charge-exchange rate coefficient as a function of the laser frequency and intensity. Moreover, shape resonances in the rate coefficients are observed as a function of the atom−ion collision energy. In a theoretical model, we can "switch" on and off the CI to further elucidate the effect of a CI on the reaction dynamics.

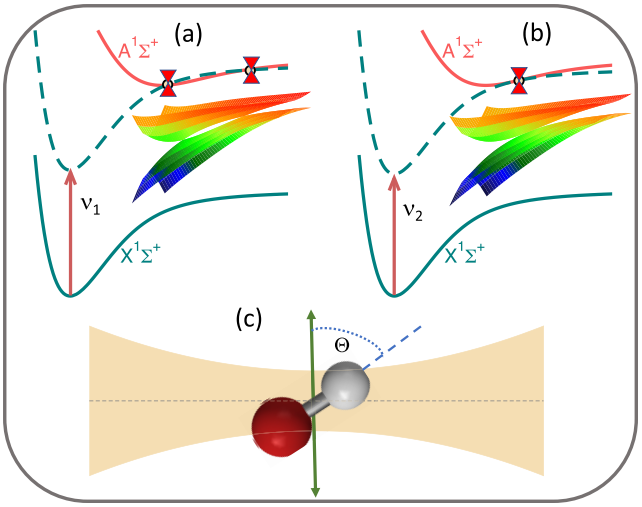

Figure 1. Schematic of the LICI-enhanced charge-exchange reaction in ultracold K+Ca^+ collisions. Panels a and b show the photon dressing of the radial diabatic potentials (line drawings) and two-dimensional adiabatic potentials of KCa^+ as functions of radial separation R and orientation θ (colored three-dimensional surfaces) with (a) two conical intersections and (b) one glancing intersection in the $R - \theta$ plane, respectively. The laser photon frequencies ν_i in panels a and b are ν_1/c = 13966 cm^{-1} and ν_2/c = 13889 cm^{-1}, respectively. Here, c is the speed of light in vacuum. Panel c shows the definition of θ, the angle between the interatomic axis (blue dashed line) connecting the atom and the ion (red and gray balls), and the direction of the linear laser polarization (green double arrow). The orange region represents the laser intensity profile (not to scale).

It is important to note that there are many examples in the literature devoted to increasing atom−ion charge-exchange reaction rates with external radiation.[29−40]

In most of these examples, the research focused on colliding neutral and ionic atoms where one or both of the colliding partners are prepared in optically excited electronic states, which led to a rich variety of exit channels. In these studies, the topology of a LICI was not invoked to explain the data, or LICIs were not even present. For example, in a recent paper in collaboration with Brown's group,[40] we demonstrated that colliding neutral ^{39}K atoms and optically excited $^{40}Ca^+$ ions confined in spatially overlapping magneto-optical and Paul traps, respectively, exhibit large charge-exchange rates. In this case, LICIs were not present. The measured charge-exchange rate coefficients were in good agreement with our theoretical estimates.

2. THEORETICAL MODEL

Ultracold collisions of K and Ca^+, both in their doublet ^2S electronic ground state, form molecular states that are superpositions of the excited singlet $A^1\Sigma^+$ and energetically lowest triplet $a^3\Sigma^+$ states,[40] where only the $A^1\Sigma^+$ component leads to radiative decay into bound states of the singlet ground $X^1\Sigma^+$ K^+Ca potential or the $K^+(^1S)$ and $Ca(^1S)$ continuum. This decay into the continuum corresponds to charge exchange with a small charge-exchange rate coefficient on the order of 10^{-14} cm^3/s.[40]

In the presence of a laser light, the charge-exchange rate coefficient can be enhanced. Figure 1 schematically shows our theoretical model of the dressed K and Ca^+ collision. The $X^1\Sigma^+$

https://doi.org/10.1021/acs.jpca.3c00242
J. Phys. Chem. A 2023, 127, 5979−5985

and $A^1\Sigma^+$ states are dressed with photons of energy $h\nu$ of the laser, allowing for additional charge-exchange processes. Here, ν is the photon frequency, and h is the Planck constant. In Figure 1(a) the potential of the $A^1\Sigma^+$ state dressed with one photon crosses the potential of the $\tilde{X}^1\Sigma^+$ state twice when the photon wavelength is 716 nm. For a photon wavelength of 720 nm in Figure 1(b), we create a glancing or Renner−Teller intersection[41] of $A^1\Sigma^+$ and $\tilde{X}^1\Sigma^+$ state potentials with a quadratic dependence on the nuclear coordinates. The colored surface plots in these panels show that the two intersections and the one glancing intersection are conical intersections in the $R - \theta$ plane for the dressed adiabatic potentials that include the atom-light coupling. In this Article, the continuous-wave laser light is linearly polarized along the space-fixed z axis, and Figure 1(c) shows the angle θ between the interatomic axis and the polarization of the laser light.

The dressed-state Hamiltonian for our system is

$$H = -\frac{\hbar^2}{2\mu_r}\frac{d^2}{dR^2} + \frac{\mathbf{L}^2}{2\mu_r R^2} + V^{\mathrm{mol}}(R) + V^{\mathrm{rad}}(\mathbf{R}) + H_{\mathrm{laser}} \tag{1}$$

where R is the internuclear separation, μ_r is the reduced mass, $\mathbf{L}$ is the molecular orbital angular momentum operator with eigenstates $|lm_l\rangle$ and projection quantum number m_l defined with respect to our space-fixed z axis, and $V^{\mathrm{mol}}(R)$ is the electronic Hamiltonian

$$V^{\mathrm{mol}}(R) = \begin{pmatrix} V_1(R) & 0 \\ 0 & V_2(R) \end{pmatrix} \tag{2}$$

where $V_1(R)$ and $V_2(R)$ are the isotropic potential energies of the singlet $X^1\Sigma^+$ and $A^1\Sigma^+$ electronic states, respectively. Their electronic wave functions will be denoted by $|1\rangle$ and $|2\rangle$. We use the potentials regarding their computations, and data tables are given in the Supporting Information. Note that for $R \to \infty$, we have $V_2(R) - V_1(R) \to \Delta \equiv +hc \times 14296.114\ \mathrm{cm}^{-1}$ derived from neutral K and neutral Ca ionization energies found in ref 42. The dissociation energy or depth and equilibrium separation of the $A^1\Sigma^+$ state potential are $D_e = hc \times 1090\ \mathrm{cm}^{-1}$ and $R_e = 12.9a_0$. Here, a_0 is the Bohr radius. The depth of the $X^1\Sigma^+$ potential is just over four times larger than that of the $A^1\Sigma^+$ state.

The fourth term in eq 1, $V^{\mathrm{rad}}(\mathbf{R})$, describes the electric dipole interaction with the laser field. In a body-fixed coordinate system, it is proportional to $\cos\theta$, where $\theta \in [0,\pi]$is the angle between the internuclear axis and the polarization of the laser field. Hence, the molecule−field interaction is anisotropic. In the rotating wave approximation,

$$V^{\mathrm{rad}}(\mathbf{R}) = -d(R)\sqrt{2\pi h\nu/V}\,\cos\theta[a^\dagger|1\rangle\langle 2| + \mathrm{h.c.}] \tag{3}$$

where $d(R)$ is the R-dependent molecular electronic transition dipole moment between the $X^1\Sigma^+$ and $A^1\Sigma^+$ states and abbreviation h.c. stands for the hermite conjugate. Finally, $H_{\mathrm{laser}} = h\nu a^\dagger a$ describes the energy in our laser field with photon creation and annihilation operators a and $a^\dagger$ in volume V, respectively. Its eigenstates are $|n\rangle$ with energy $nh\nu$ for non-negative integers or photon numbers n. The operator $V^{\mathrm{rad}}(\mathbf{R})$ has nonzero matrix elements between states that differ by one photon number. Effects of the permanent dipole moments of the $X^1\Sigma^+$ and $A^1\Sigma^+$ states are neglected. They do not lead to charge exchange. We use the transition dipole moment from ref 40. See the Supporting Information for a description and a data table. Potential energy curves, spectroscopic constants, and transition electric dipole moments of K^+Ca were also determined and analyzed in ref 43.

For coupled-channels calculations, we use the basis $|i; lm_l; n\rangle \equiv |i\rangle|lm_l\rangle|n\rangle$ with $i = 1, 2$. In this basis, $\mathbf{L}^2$, V_{mol}, and H_{laser} are diagonal. Only, $V^{\mathrm{rad}}(\mathbf{R})$ couples basis functions with matrix elements

$$\langle 1; lm_l; n+1|V^{\mathrm{rad}}(\mathbf{R})|2; l'm_l'; n\rangle = -d(R)\sqrt{\frac{2\pi I}{c}}\sqrt{\frac{2l'+1}{2l+1}}\,C^{lm_l}_{10,l'm_l'}C^{l0}_{10,l'0} \tag{4}$$

where I is the laser intensity and $C^{jm}_{j_1m_1,j_2m_2}$ are Clebsch−Gordan coefficients. For our laser polarization $m_l' = m_l$ and the matrix element is only nonzero when $l + l'$ is odd. The dressed state picture, pioneered by Cohen-Tannoudji et al.[44] and as used here, is for large photon number $n \gg 1$ equivalent to Floquet theory based on a classical time-dependent description of light. For $n \gg 1$, it is appropriate to replace the photon number dependence of the matrix element in eq 4 by the mean photon number (per unit area) in the laser and thus by laser intensity I as it is proportional to the mean photon number. As we will show, the change in photon number due to the molecular processes is small even at our largest laser intensities.

The charge-exchange rate coefficient from $|1\rangle$ with n photons and ultracold collision energy E is given by

$$K = \frac{\hbar\pi}{\mu_r k}\sum_{l,l'=0}^{l_{\max}}\sum_{m_l}\sum_{n'=n-\delta n}^{n+\delta n}|T_{2,l'm_l,n'\leftarrow 1,l,m_l,n}|^2 \tag{5}$$

where $k = \sqrt{2\mu_r E/\hbar^2}$ is the collisional wave vector, m_l runs from $-\min(l, l')$ to $\min(l, l')$, and $\hbar$ is the reduced Planck constant. The quantities $T_{f\leftarrow i}$ are T-matrix elements obtained from scattering solutions of eq 1, where the photon numbers changes by no more that $\delta n = 1$ or 2, and partial waves l from 0 to $l_{\max} = 6$ are coupled, sufficient for convergence at collision energies E up to $k \times 1$ mK and laser intensities up to 10^8 W/cm^2. Here, k is the Boltzmann constant. We find that the main contribution to K comes from T-matrix elements with $n' = n + 1$, corresponding to the transition $|1\rangle + nh\nu \to |2\rangle + (n+1)h\nu$.

In this paper, we focus on photon energies between $hc \times 13600\ \mathrm{cm}^{-1}$ and $\Delta = hc \times 14296.114\ \mathrm{cm}^{-1}$, to ensure the presence of up to two LICIs between the $X^1\Sigma^+$ and $A^1\Sigma^+$ potentials, as shown in Figure 1. The LICIs are best visible in the surface graphs of Figure 1(a) and (b) corresponding to the eigenvalues of operator $V^{\mathrm{mol}}(R) + V^{\mathrm{rad}}(\mathbf{R})$ as functions of R and θ. The LICIs occur at $\theta = \pi/2$ with separations R_1 and R_2, where $R_1 \le R_2$. For the Renner−Teller intersection, $R_1 = R_2 > R_e$.

3. RESULTS AND DISCUSSIONS

3.1. Interference Patterns between Pathways around Two LICIs. We begin by investigating the effect of LICIs on rate coefficients of the charge-exchange reaction K_{LICI} by calculating the rate coefficient around an $hc \times 800\ \mathrm{cm}^{-1}$ range of photon energies below the difference in dissociation energy of the $X^1\Sigma^+$ and $A^1\Sigma^+$ states. A representative example is shown in Figure 2(a) for a collision energy of $E/k = 7\ \mu$K and a laser intensity of 10^8 W/cm^2. The laser wavenumber is increased from $\nu/c = 13600$ to $14296.114\ \mathrm{cm}^{-1} = \Delta/hc$, where our system goes from having no LICI to one where two LICIs exist

https://doi.org/10.1021/acs.jpca.3c00242
J. Phys. Chem. A 2023, 127, 5979−5985

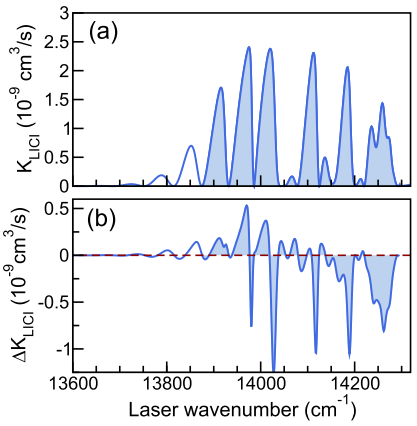

Figure 2. (a) Charge-exchange rate coefficient K_{LICI} as a function of laser wavenumber at a collision energy of E/k = 7 μK and a laser intensity of $I = 10^8$ W/cm^2. The shaded light-blue region indicates the frequency region where interferences between pathways around the two conical intersections occur. (b) The difference $\Delta K_{LICI} = K_{no-LICI} - K_{LICI}$ as a function of laser wavenumber at E/k = 7 μK and $I = 10^8$ W/cm^2. Here, $K_{no-LICI}$ and K_{LICI} are charge-exchange rate coefficients computed without and with conical intersections, respectively.

between the $A^1\Sigma^+$ and $\tilde{X}^1\Sigma^+$ potentials. We observe regular and irregular Stückelberg oscillations, where the rate coefficient alternates between near zero values and maxima as a function of ν. Below ν/c = 13600 cm^{-1} the light-induced charge-exchange rate coefficient is below $\sim 10^{-14}$ cm^3/s and radiative decay studied in ref 40 becomes the dominant means for charge exchange. For $h\nu > \Delta$ the light-induced rate coefficient K_{LICI} is negligibly small as transition $|1\rangle + nh\nu \rightarrow |2\rangle + (n+1)h\nu$ is energetically forbidden.

For photon energies between $hc \times$ 13600 cm^{-1} and $hc \times$ 13896 cm^{-1} we observe Stückelberg oscillations with increasing amplitude, corresponding to cases where we only have avoided crossings between $A^1\Sigma^+$ and $\tilde{X}^1\Sigma^+$ potentials. The amplitude of the oscillations increases because the avoided crossing between the potentials become narrower. Starting from laser energies $hc \times$ 13896 cm^{-1}, shaded in Figure 2(a), two conical intersections are present, and the oscillation pattern of K_{LICI} is significantly distorted or irregular due to interferences between multiple pathways around the two conical intersections.

To support our claim that the irregular Stückelberg oscillations are due to LICIs, we first analyze the charge-exchange rate coefficient for selected laser frequencies in this frequency window. Specifically, we analyze perturbative transition matrix elements between scattering wave functions in channels $|1; lm_l; n\rangle$ and $|2; l'm_l'; n+1\rangle$ as a function of laser frequency and locate the origin of the complex constructive and destructive interferences corresponding to large and small charge-exchange rate coefficients. We define the *partial* matrix element or integral

$$M(R) = \int_0^R \mathrm{d}r\ \psi_X(r)\ d(r)\ \phi_A(r) \tag{6}$$

where real-valued $\phi_A(r)$ is the single-channel $l = 0$ radial scattering wave function for the $A^1\Sigma^+$ potential at initial collision energy $E_{initial}$ and real-valued $\psi_X(r)$ is the single-channel $l = 1$ radial scattering wave function for the $\tilde{X}^1\Sigma^+$ potential at final collision energy $E_{final} = \Delta - h\nu + E_{initial}$. For weak laser intensities, the charge-exchange rate coefficient K_{LICI} is proportional to the square of $M(R)$ for $R \rightarrow \infty$. Constructive or destructive interference implies large or small $|M(R \rightarrow \infty)|$, respectively.

We begin the analysis by showing the rate coefficient K_{LICI} at a collision energy of E/k = 1 μK in Figure 3 on a logarithmic scale. The interference pattern is similar to that observed in Figure 2 with a larger collision energy. Figure 4 then shows the partial matrix element $M(R)$ and the integrand $\psi_X(R)\ d(R)\ \phi_A(R)$ as functions of R for an initial collision energy of $E_{initial}$ = 1 μK when the wavenumbers of the dressing laser are ν/c = 14196, 14056, and 13996 cm^{-1}, respectively. The product $d(R)\ \phi_A(R)$ is the same for the three cases, and only $\psi_X(R)$ changes.

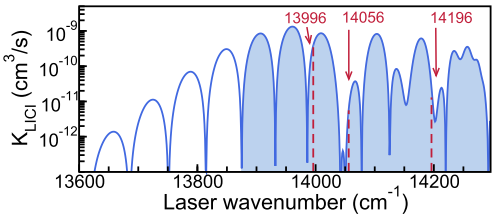

Figure 3. Charge-exchange rate coefficient K_{LICI} as a function of laser wavenumber at E/k = 1 μK and $I = 10^8$ W/cm^2. The shaded light-blue region again indicates the frequency region where interferences between pathways around the two conical intersections occur. Wavenumbers 13996, 14056, and 14196 cm^{-1} with dashed red lines mark dressing conditions, leading to either constructive or near destructive interference.

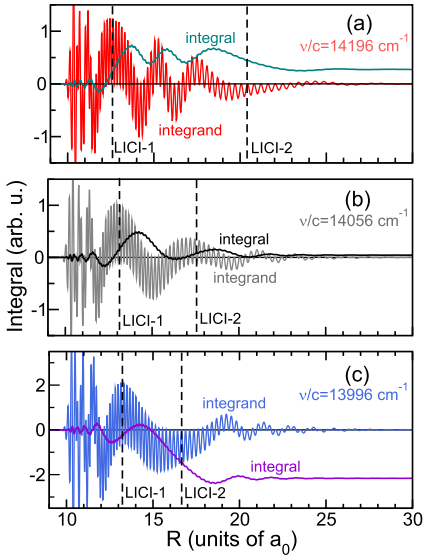

Figure 4. Explanation of the irregular Stückelberg oscillations in the K + Ca$^+$ charge-exchange rate coefficient at a collision energy of $k \times 1$ μK shown in Figure 3 when the dressed-state potentials have two LICIs. Panels a–c show the integrand and partial integral of vibrationally averaged electronic transition dipole moments as functions of atom–atom separation R for laser wavenumbers ν/c = 14196, 14056, and 13996 cm^{-1}, respectively. The vertical black dashed lines labeled LICI-1 and LICI-2 in each panel correspond to the KCa$^+$ separations of the LICIs. The scales on the y axes of the panels are different and should not be compared.

For the largest photon energy, shown in panel a, the system has two well-separated conical intersections located at separations R_1 and R_2 with $R_1 < R_2$. They are labeled LICI-1

https://doi.org/10.1021/acs.jpca.3c00242
J. Phys. Chem. A 2023, 127, 5979–5985

and LICI-2 in the figure. We also observe that the integrand is a rapidly oscillating function with R and that it approaches zero for large R as $d(R) \to 0$ for $R \to \infty$. Hence, we expect that cancellations but also nonzero averages will occur in the calculation of $M(R)$. Near $R = R_1$ and R_2, where the local kinetic energies for $\tilde{X}^1\Sigma^+$ and $A^1\Sigma^+$ states are close to equal, however, the oscillations in the integrand occur around a nonzero average and, indeed, for R near R_1 the integral is seen to rapidly increase. Near $R = R_2$ the integral decreases somewhat. For all other R, $M(R)$ oscillates around a stable value. Thus, we realize that for $\nu/c = 14196$ cm^{-1} and $R \to \infty$, the contributions to $M(R)$ from the two LICIs partially cancel.

For the data at $\nu/c = 14056$ cm^{-1} in Figure 4(b) the contributions from the two LICIs nearly cancel each other. There is destructive interference between the LICIs. For the data in panel c and $\nu/c = 13996$ cm^{-1}, the radial separations of the two CIs are the closest of all three cases and the contributions from the two LICIs are harder to separate. Still, the contribution to $M(R)$ near LICI-1 averages to near zero, while the contribution from LICI-2 is large. From similar figures at other kinetic energies and laser frequencies, not shown, we can understand the patterns seen in Figure 2(a) as a function of laser frequency.

We also performed a second type of analysis to confirm that the light-induced conical intersections influence the charge-exchange process. We "removed" the conical intersections by replacing the anisotropic θ dependence in eq 3 with an isotropic one. In fact, we made the substitution

$$\cos\theta \to \frac{1}{\sqrt{3}} \tag{7}$$

in eq 3. The molecule−field interaction is now isotropic and only couples channels with the same partial wave l and m_l quantum numbers.

Figure 2(b) shows the difference of the charge-exchange rate coefficients $K_{\text{no-LICI}}$ and K_{LICI} as a function of laser frequency at $E/k = 1$ μK and $I = 10^8$ W/cm^2. Here, $K_{\text{no-LICI}}$ and K_{LICI} correspond to rate coefficients computed without and with conical intersections, respectively. The difference in rate coefficients can be of the same order of magnitude as K_{LICI} and be as large as $\pm 10^{-9}$ cm^3/s in the frequency window where the conical interactions are present. For ultracold atom and ion experiments, a rate coefficient on the order of 10^{-9} cm^3/s is large and easily detectable.

Finally, we examine charge-exchange rate coefficients between K and Ca^+ as functions of collision energy E at $\nu/c = 13960$ cm^{-1} and laser intensities of 10^6, 10^7, and 10^8 W/cm^2. We remain in the ultracold collision energy domain below $k \times 1$ mK. This case corresponds to a situation where K_{LICI} is close to maximal when $E \to 0$ and the pair of interfering conical intersections are located close together. Figure 5(a) shows rate coefficients K_{LICI} where the LICIs present. We observe that both wide and narrow resonance features are present. Further analysis has shown that these resonances are due to shape resonances behind a l -wave centrifugal barrier of the long-range $-C_4/R^4 + \hbar^2 l(l+1)/(2\mu_r R^2)$ potential between a neutral atom and an ionic atom. Here, C_4 is the polarization coefficient proportional to the static polarizability of the K atom. These resonances significantly enhance the charge-exchange process. A broader resonance has an energy closer to the top of the corresponding centrifugal barrier. The rate coefficients increase approximately linearly with laser intensity,

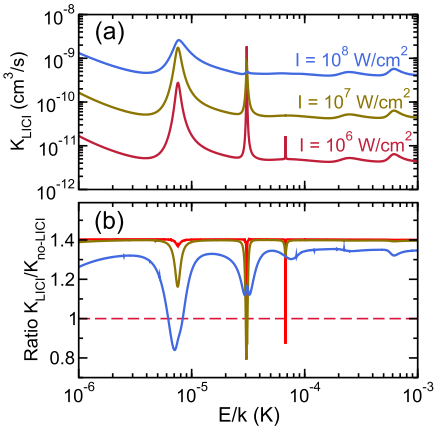

Figure 5. Charge-exchange rate coefficient K_{LICI} computed with the CIs present (panel a) and the ratio $K_{\text{LICI}}/K_{\text{no-LICI}}$ (panel b) as functions of atom−ion collision energy at laser wavenumber $\nu/c = 13960$ cm^{-1} and at laser intensities of $I = 10^6$ W/cm^2 (red curve), 10^7 W/cm^2 (gold), and 10^8 W/cm^2 (blue).

although for the largest intensity of 10^8 W/cm^2 deviations are visible. For example, the resonances have noticeably broadened, which can be used as a signal that CIs are present.

Figure 5(b) shows the ratio $K_{\text{LICI}}/K_{\text{no-LICI}}$ of $\nu/c = 13960$ cm^{-1} rate coefficients K_{LICI} and $K_{\text{no-LICI}}$ calculated when the LICIs are and are not present, respectively. We observe that for the smaller laser intensities the ratio is about 1.4 independent of collision energy and laser intensity except near the shape resonances. At the higher laser intensity of 10^8 W/cm^2 the background value of the ratio of rate coefficients also changes in a measurable way, although the width and strength of the resonances are again affected more dramatically.

3.2. In Summary. We have computed charge-exchange rate coefficients of colliding K atoms and Ca^+ ions confined in hybrid atom−ion traps at ultracold temperatures in the presence of a near resonant laser beam that initiates nonadiabatic coupling between the ground and first excited electronic potential energy surfaces of this ionic system. The underlying time-independent coupled-channels calculations allowed us to treat the nonadiabatic nuclear dynamics, dominated by two light-induced conical intersections, exactly. In particular, our state-of-the-art calculations showed the presence of interference between pathways around two conical intersections. We have shown that these laser-induced conical intersections can significantly increase the atom−ion chemical reactivity at ultracold collision energies and relatively low intensities of the dressing laser. The expected rate coefficients should be easily detectable in the current experimental setups. We also investigated charge exchange when the conical intersections were removed. The results of those studies showed that the conical intersections lead to noticeable differences in the reactive charge-exchange reaction.

■ ASSOCIATED CONTENT

Supporting Information

The Supporting Information is available free of charge at https://pubs.acs.org/doi/10.1021/acs.jpca.3c00242.

Electronic structure of the KCa^+ molecule, including tabulated values of potential energy curves and electric transition dipole moments (PDF)

https://doi.org/10.1021/acs.jpca.3c00242
J. Phys. Chem. A 2023, 127, 5979−5985

AUTHOR INFORMATION

Corresponding Author

Svetlana Kotochigova − *Department of Physics, Temple University, Philadelphia, Pennsylvania 19122, United States;* orcid.org/0000-0003-0580-3788; Email: skotoch@temple.edu

Authors

Hui Li − *Department of Physics, Temple University, Philadelphia, Pennsylvania 19122, United States;* Present Address: JILA, University of Colorado, Boulder, Colorado 80309, USA

Ming Li − *Department of Physics, Temple University, Philadelphia, Pennsylvania 19122, United States;* Present Address: Atom Computing, Inc.

Alexander Petrov − *Department of Physics, Temple University, Philadelphia, Pennsylvania 19122, United States*

Eite Tiesinga − *Joint Quantum Institute, National Institute of Standards and Technology and University of Maryland, Gaithersburg, Maryland 20899, United States*

Complete contact information is available at: https://pubs.acs.org/10.1021/acs.jpca.3c00242

Notes

The authors declare no competing financial interest.

ACKNOWLEDGMENTS

Work at Temple University is supported by the U.S. Air Force Office of Scientific Research Grants No. FA9550-21-1-0153 and No. FA9550-19-1-0272 and the NSF Grant No. PHY-1908634.

REFERENCES

(1) Born, M.; Oppenheimer, R. Zur Quantentheorie der Molekeln. *Ann. Phys.* **1927**, *389*, 457.

(2) Baer, M. *Beyond Born-Oppenheimer: Electronic Nonadiabatic Coupling Terms and Conical Intersections*; John Wiley & Sons: New York, 2006.

(3) Domcke, W.; Yarkony, D.; Köppel, H. *Conical Intersections: Electronic Structure, Dynamics & Spectroscopy*; Advanced Series in Physical Chemistry Singapore, 2004; Vol. *15*.

(4) Domcke, W.; Yarkony, D.; Köppel, H. *Conical Intersections: Theory, Computation and Experiment*; Advanced Series in Physical Chemistry; World Scientific Publishing Company, 2011; Vol. *17*.

(5) Zhu, X.; Yarkony, D. R. Non-adiabaticity: the importance of conical intersections. *Mol. Phys.* **2016**, *114*, 1983−2013.

(6) Klessinger, M.; Michl, J. *Excited States and the Photochemistry of Organic Molecules*; VCH: New York, 1995.

(7) Peleg, O.; Bartal, G.; Freedman, B.; Manela, O.; Segev, M.; Christodoulides, D. N. Conical Diffraction and Gap Solitons in Honeycomb Photonic Lattices. *Phys. Rev. Lett.* **2007**, *98*, 103901.

(8) Leone, R.; Lévy, L. P.; Lafarge, P. Cooper-Pair Pump as a Quantized Current Source. *Phys. Rev. Lett.* **2008**, *100*, 117001.

(9) Moiseyev, N.; Šindelka, M.; Cederbaum, L. S. Laser-induced conical intersections in molecular optical lattices. *J. Phys. B* **2008**, *41*, 221001.

(10) Moiseyev, N.; Šindelka, M. The effect of polarization on the light-induced conical intersection phenomenon. *J. Phys. B* **2011**, *44*, 111002.

(11) Šindelka, M.; Moiseyev, N.; Cederbaum, L. S. Strong impact of light-induced conical intersections on the spectrum of diatomic molecules. *J. Phys. B* **2011**, *44*, 045603.

(12) Szidarovszky, T.; Halász, G. J.; Császár, A. G.; Cederbaum, L. S.; Vibók, Á. Conical intersections induced by quantum light: Field-dressed spectra from the weak to the ultrastrong coupling regimes. *J. Phys. Chem. Lett.* **2018**, *9*, 6215−6223.

(13) Szidarovszky, T.; Halász, G. J.; Császár, A. G.; Cederbaum, L. S.; Vibók, Á. Direct signatures of light-induced conical intersections on the field-dressed spectrum of Na_2. *J. Phys. Chem. Lett.* **2018**, *9*, 2739−2745.

(14) Demekhin, P. V.; Chiang, Y.; Cederbaum, L. S.; Resonant, A. uger decay of core-excited C*O molecules in intense x-ray laser fields. *Phys. Rev. A* **2011**, *84*, 033417.

(15) Demekhin, P. V.; Cederbaum, L. S. Resonant Auger decay of core-excited CO molecules in intense x-ray laser pulses: the O(1s→π^*) excitation. *J. Phys. B* **2013**, *46*, 164008.

(16) Wallis, A. O. G.; Hutson, J. M. Optically induced conical intersections in traps for ultracold atoms and molecules. *Phys. Rev. A* **2011**, *84*, 051402.

(17) Wüster, S.; Eisfeld, A.; Rost, J. M. Conical Intersections in an Ultracold Gas. *Phys. Rev. Lett.* **2011**, *106*, 153002.

(18) Tóth, A.; Csehi, A.; Halász, G. J.; Vibók, A. Photodissociation dynamics of the LiF molecule: Two- and three-state descriptions. *Phys. Rev. A* **2019**, *99*, 043424.

(19) Halász, G. J.; Vibók, A.; Moiseyev, N.; Cederbaum, L. S. Nuclear-wave-packet quantum interference in the intense laser dissociation of the D_2^+ molecule. *Phys. Rev. A* **2013**, *88*, 043413.

(20) Halász, G. J.; Vibók, Á.; Cederbaum, L. S. Direct signature of light-induced conical intersections in diatomics. *J. Phys. Chem. Lett.* **2015**, *6*, 348−354.

(21) Csehi, A.; Halász, G. J.; Cederbaum, L. S.; Vibók, A. Towards controlling the dissociation probability by light-induced conical intersections. *Faraday Discuss.* **2016**, *194*, 479−493.

(22) Csehi, A.; Halász, G. J.; Cederbaum, L. S.; Vibók, A. Competition between light-Induced and intrinsic nonadiabatic phenomena in diatomics. *J. Phys. Chem. Lett.* **2017**, *8*, 1624−1630.

(23) Csehi, A.; Vendrell, O.; Halász, G. J.; Vibók, Á. Competition between collective and individual conical intersection dynamics in an optical cavity. *New J. Phys.* **2022**, *24*, 073022.

(24) Kim, J.; Tao, H.; White, J. L.; Petrovic, V. S.; Martinez, T. J.; Bucksbaum, P. H. Control of 1, 3-cyclohexadiene photoisomerization using light-induced conical intersections. *J. Phys. Chem. A* **2012**, *116*, 2758−2763.

(25) Corrales, M.; González-Vázquez, J.; Balerdi, G.; Solá, I. R.; De Nalda, R. Bañares, L. Control of ultrafast molecular photodissociation by laser-field-induced potentials. *Nat. Chem.* **2014**, *6*, 785−790.

(26) Natan, A.; Ware, M. R.; Prabhudesai, V. S.; Lev, U.; Bruner, B. D.; Heber, O.; Bucksbaum, P. H. Observation of Quantum Interferences via Light-Induced Conical Intersections in Diatomic Molecules. *Phys. Rev. Lett.* **2016**, *116*, 143004.

(27) Kübel, M.; Spanner, M.; Dube, Z.; Naumov, A. Y.; Chelkowski, S.; Bandrauk, A. D.; Vrakking, M. J.; Corkum, P. B.; Villeneuve, D.; Staudte, A. Probing multiphoton light-induced molecular potentials. *Nat. Commun.* **2020**, *11*, 2596.

(28) Thomas, R.; Roberts, K.; Tiesinga, E.; Wade, A.; Blakie, P.; Deb, A. Kjærgaard, N. Multiple scattering dynamics of fermions at an isolated p-wave resonance. *Nat. Commun.* **2016**, *7*, 12069.

(29) Vitlina, R. Z.; Chaplik, A. V.; Entin, M. V. Nonresonant charge transfer in the field of an intense light wave. *Zh. Eksp. Teor. Fiz.* **1974**, *67*, 1667−1673.

(30) Copeland, D. A.; Tang, C. L. Photon-assisted nonresonant charge exchange: A simple molecular model. *J. Chem. Phys.* **1976**, *65*, 3161.

(31) Copeland, D. A.; Tang, C. L. On the optimal photon energy for photon-assisted nonresonant charge exchange. *J. Chem. Phys.* **1977**, *66*, 5126.

(32) George, T. F. Laser-Stimulated Molecular Dynamics and Rate Processes. *J. Phys. Chem.* **1982**, *86*, 10.

(33) Ho, T.-S.; Laughlin, C.; Chu, S.-I Laser-assisted charge-transfer reactions (Li^{3+}+H): Coupled dressed- quasimolecular-state approach. *Phys. Rev. A* **1985**, *32*, 122.

(34) Hsu, Y. P.; Kimura, M.; Olson, R. E. Laser-assisted charge-transfer collisions: K^+ + Na. *Phys. Rev. A* **1985**, *31*, 576.

(35) Sussman, B. J.; Townsend, D.; Ivanov, M. Y.; Stolow, A. Dynamic Stark Control of Photochemical Processes. *Science* **2006**, *314*, 278.
(36) Hall, F. H. J.; Aymar, M.; Bouloufa-Maafa, N.; Dulieu, O.; Willitsch, S. Light-Assisted Ion-Neutral Reactive Processes in the Cold Regime: Radiative Molecule Formation versus Charge Exchange. *Phys. Rev. Lett.* **2011**, *107*, 243202.
(37) Petrov, A.; Makrides, C.; Kotochigova, S. Laser controlled charge-transfer reaction at low temperatures. *J. Chem. Phys.* **2017**, *146*, 084304.
(38) Mills, M.; Puri, P.; Li, M.; Schowalter, S. J.; Dunning, A.; Schneider, C.; Kotochigova, S.; Hudson, E. R. Engineering Excited-State Interactions at Ultracold Temperatures. *Phys. Rev. Lett.* **2019**, *122*, 233401.
(39) Li, M.; Mills, M.; Puri, P.; Petrov, A.; Hudson, E. R.; Kotochigova, S. Excitation-assisted nonadiabatic charge-transfer reaction in a mixed atom-ion system. *Phys. Rev. A* **2019**, *99*, 062706.
(40) Li, H.; Jyothi, S.; Li, M.; Kłos, J.; Petrov, A.; Brown, K. R.; Kotochigova, S. Photon-mediated charge exchange reactions between ^{39}K atoms and $^{40}Ca^{+}$ ions in a hybrid trap. *Phys. Chem. Chem. Phys.* **2020**, *22*, 10870−10881.
(41) Yarkony, D. R. Conical Intersections: Diabolical and Often Misunderstood. *Acc. Chem. Res.* **1998**, *31*, 511−518.
(42) Kramida, A.; Ralchenko, Y.; Reader, J. *team, N. A. NIST Atomic Spectra Database (ver. 5.0)*.http://physics.nist.gov/asd.
(43) Zrafi, W.; Ladjimi, H.; Said, H.; Berriche, H.; Tomza, M. Ab initio electronic structure and prospects for the formation of ultracold calcium-alkali-metal-atom molecular ions. *New J. Phys.* **2020**, *22*, 073015.
(44) Cohen-Tannoudji, C.; Dupont-Roc, J.; Grynberg, G. *Atom-Photon Interactions: Basic Processes and Applications*; John Wiley & Sons: New York, 1992.

https://doi.org/10.1021/acs.jpca.3c00242
J. Phys. Chem. A 2023, 127, 5979−5985